Preprint Cambridge Centre for Computational Chemical Engineering ISSN 1473 – 4273

Modelling particle mass and particle number emissions during the active regeneration of diesel particulate filters

Chung Ting Lao[1], Jethro Akroyd[1], Nickolas Eaves[1], Alastair Smith[2], Neal Morgan[2], Amit Bhave[3], Markus Kraft[1,4,5]

released: 20 August 2018

[1] Department of Chemical Engineering
and Biotechnology
University of Cambridge
Philippa Fawcett Drive
Cambridge, CB3 0AS
United Kingdom
E-mail: mk306@cam.ac.uk

[2] Shell Projects & Technology
Brabazon House
Threapwood Road
Manchester, M22 0RR
United Kingdom

[3] CMCL Innovations
Sheraton House
Cambridge, CB3 0AX
United Kingdom

[4] School of Chemical and
Biomedical Engineering
Nanyang Technological University
62 Nanyang Drive
637459
Singapore

[5] Cambridge Centre for Advanced Research
and Education in Singapore (CARES)
CREATE Tower, 1 Create Way
138602
Singapore

Preprint No. 208

UNIVERSITY OF CAMBRIDGE

Keywords: c4e, preprint, Diesel Particulate Filter (DPF), Regeneration, Population balance model, Unit collector, Emissions

Edited by
Computational Modelling Group
Department of Chemical Engineering and Biotechnology
University of Cambridge
Philippa Fawcett Drive
Cambridge CB3 0AS
United Kingdom

E-Mail: c4e@cam.ac.uk
World Wide Web: http://como.ceb.cam.ac.uk/

Abstract

A new model has been developed to describe the size-dependent effects that are responsible for transient particle mass (PM) and particle number (PN) emissions observed during experiments of the active regeneration of Diesel Particulate Filters (DPFs). The model uses a population balance approach to describe the size of the particles entering and leaving the DPF, and accumulated within it. The population balance is coupled to a unit collector model that describes the filtration of the particles in the porous walls of the DPF and a reactor network model that is used to describe the geometry of the DPF. Two versions of the unit collector model were investigated. The original version, based on current literature, and an extended version, developed in this work, that includes terms to describe both the non-uniform regeneration of the cake and thermal expansion of the pores in the DPF. Simulations using the original unit collector model were able to provide a good description of the pressure drop and PM filtration efficiency during the loading of the DPF, but were unable to adequately describe the change in filtration efficiency during regeneration of the DPF. The introduction of the extended unit collector description enabled the model to describe both the timing of particle breakthrough and the final steady filtration efficiency of the hot regenerated DPF. Further work is required to understand better the transient behaviour of the system. In particular, we stress the importance that future experiments fully characterise the particle size distribution at both the inlet and outlet of the DPF.

Highlights

- Modelling study on filtration behaviour of Diesel Particulate Filter (DPF) during active regeneration
- One of the first comparison between filtration model and experimental data for DPF active regeneration
- Extended state-of-the-art filtration model to improve description of experimental observation

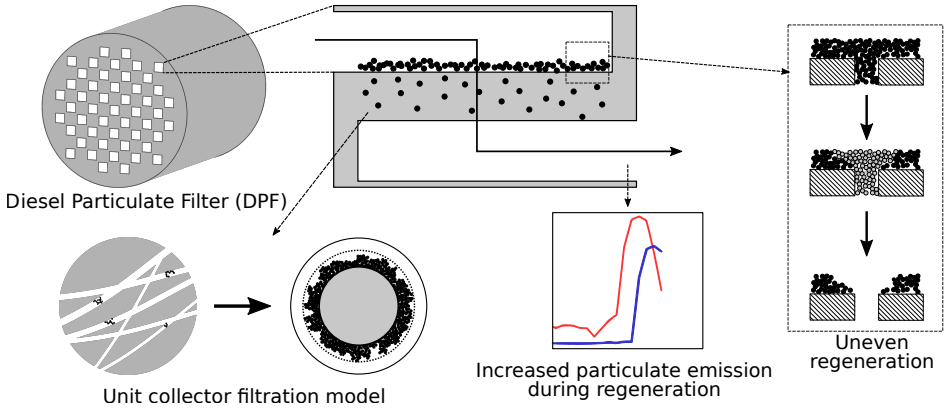

Contents

1 Introduction

Particulate emissions are a major concern for diesel engine technology due to their negative impact on human health [20] and the environment [22]. Diesel Particulate Filters (DPFs) are installed in diesel engine systems in order to limit particulate emissions to the atmosphere. Most DPFs have a Wall Flow Monolith (WFM) structure. A WFM consists of large number of parallel channels with a porous wall substrate. The ends of the channels are alternately plugged. As a result, exhaust is forced to flow through the porous walls between the channels. Particles suspend in the exhaust are filtered by the porous wall.

As the porous wall is loaded with particles, fewer particles are able to penetrate the wall and incoming particles start to form a filter cake on the wall-channel interface. The blockage of the pores and the formation of the cake lead to an increase in the filtration efficiency at the expense of a higher pressure drop across the DPF. High backpressure is detrimental to the combustion efficiency of the engine. For this reason, DPFs are periodically regenerated to burn off the trapped particles and reduce the pressure drop caused by the DPF. There are two common regeneration strategies: active and passive regeneration. Active regeneration involves temporarily raising the temperature in the DPF to above 500°C such that trapped carbonaceous particles are oxidised [5]. Typically, active regeneration is required every 300–800 km journey, lasts 5–15 min and leads to 2–3% additional fuel consumption [2]. This can be avoided by using passive regeneration. Passive regeneration catalytically converts nitrogen monoxide to nitrogen dioxide, a powerful oxidant, which can continuously oxidise trapped carbonaceous particles at typical exhaust temperatures (300 °C) [25]. However, the reliance on NOx means that passive regeneration is not always sufficient under all engine operating conditions [12].

Significant transient particulate emissions have been observed in experiments investigating active regeneration events. Various mechanisms have been proposed in the literature to explain these observations. Firstly the removal of particles from the cake layer and from inside the porous walls leads to a lower filtration efficiency. Secondly, the high temperature during active regeneration has been suggested to lead to expansion of the porous wall, leading to a further decrease in filtration efficiency [23]. Thirdly, if the active regeneration is initiated by fuel injection into the engine cylinder towards the end of expansion stroke, the particle flow into the exhaust system could change significantly due to different operating conditions in the engine [17]. Fourthly, additional particles may also be formed upstream of the inlet of the DPF if extra fuel is injected into the tailpipe [27]. It was hypothesised that particle breakthrough could be a result of fragmentation of the trapped particles during rapid oxidation events, which then proceed to escape the DPF [1]. Last but not least, semi-volatile particles can be emitted during active regeneration in addition to solid particles [12]. Catalysts in the after-treatment system can oxidise sulphur dioxide to form sulphur trioxide in the engine-out exhaust. Sulphuric acid is then formed from sulphur trioxide and water vapour. Nucleation of semi-volatile particles can occur when the gaseous sulphuric acid leaves the exhaust system.

The unit collector filtration model has been developed and widely adopted to simulate DPF filtration performance. However it has only been experimentally validated at low-temperature conditions [18]. Modelling studies on active regeneration of DPFs have

mainly focused on the thermal behaviour of the system [for example 28]. The filtration efficiency during regeneration has rarely been compared with experimental results [26]. Investigations on the filtration performance of DPFs under regenerating conditions are mostly experimental [2]. This leaves a gap in the understanding of the filtration behaviour of regenerating DPFs, which is crucial due to more stringent emission standards and increasing attention on Real Driving Emissions (RDE) [24].

In this study, the unit collector filtration model is coupled to a reactor network model that allows detailed treatment of the chemistry (for example, allowing the use of user-supplied chemical mechanisms with arbitrary number of species and reactions) , straightforward treatment of the geometry and a population balance model to describe the particulate matter. The model is applied to describe the particle mass and particle number filtration efficiency of a Diesel Particulate Filter (DPF) during active regeneration of the system studied experimentally by Rothe et al. [23]. The unit collector model was extended to describe additional phenomena including thermal pore expansion in the porous wall and the non-uniform dissolution of the particle cake layer. The performance of the original model and the extended model are evaluated against experimental data. Further areas for development are discussed.

2 Model description

2.1 Governing equations

The model describes the porous wall between a representative pair of inlet and outlet channels. It necessarily assumes that the inlet conditions are identical for all DPF channels, which is a common modelling choice [26]. The channels are discretised in the axial direction. The porous wall is discretised both in the axial direction and the through-wall direction. This choice of spatial discretisation is commonly adopted since it is computational efficient without incurring a significant loss of precision [26]. This is shown schematically in Fig. 1. Each volume element is treated as a Perfectly Stirred Reactor (PSR). The ideal gas law is chosen as the equation of state for the gas phase.

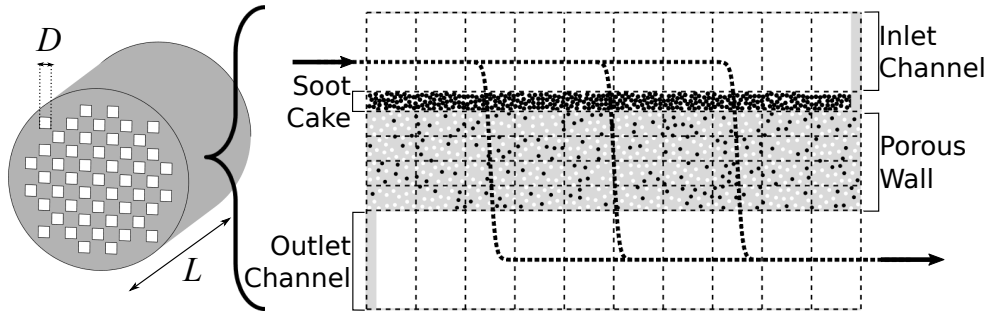

Figure 1: *Schematic spatial discretisation of the single-channel DPF model. Each volume element outlined by dashed lines is represented by a Perfectly Stirred Reactor (PSR).*

The relationship between the pressure and the velocity of the gas in the channels is governed by Bernoulli's equation,

$$P_{\text{in}} + \frac{1}{2}\rho_{\text{in}} u_{\text{in}}^2 + \frac{F\mu\Delta L}{D^2} u_{\text{in}} = P_{\text{out}} + \frac{1}{2}\rho_{\text{out}} u_{\text{out}}^2, \tag{1}$$

where P, ρ and u denote the pressure, density and axial velocity respectively. The subscripts "in" and "out" stand for inlet and outlet conditions. The friction factor F for a square channel is 28.454 [8]. The viscosity μ of the gas is approximated as that of air. The length between inlet and outlet and the side length of the channel cross-section are represented by ΔL and D respectively. The gas flow through the cake and the wall is calculated using Darcy's Law:

$$P_{\text{in}} - P_{\text{out}} = \frac{\mu v L_{\text{pw}}}{\kappa}, \tag{2}$$

where v is the through-wall velocity, L_{pw} is the thickness of the porous medium and κ is the permeability of the porous medium. Diffusive mass transport between volume elements is neglected in the model since this phenomena is only important for uncontrolled regeneration [13], whereas the particular system in this study underwent controlled regeneration. The number of moles n of gas-phase species γ in volume element i is governed by eq. (3) which considers inflow/outflow and chemical reaction:

$$\frac{\mathrm{d}n_{\gamma,i}}{\mathrm{d}t} = \sum_{\forall \text{in}} \frac{\dot{m}_{\text{in}} Y_{\gamma,\text{in}}}{M_\gamma} - \sum_{\forall \text{out}} \frac{\dot{m}_{\text{out}} Y_{\gamma,i}}{M_\gamma} + V_i \sum_{\forall w} \nu_{\gamma,w} r_{w,i}. \tag{3}$$

The inlet and outlet gas mass flow are denoted as $\dot{m}_{\text{in}}$ and $\dot{m}_{\text{out}}$ respectively. Y_γ and M_γ are the mass fraction and the molecular mass of species γ. The rate and stoichiometric coefficients of reaction w are denoted as $r_{w,i}$ and $\nu_{\gamma,w}$ respectively. In this study, it is assumed that the gas inside the porous wall is always at the wall temperature. In addition to advection and chemical reactions, the gas in the channels exchanges heat with the porous wall via an overall heat transfer coefficient accounting for convective heat transfer. Heat conduction is considered in the cake layer and the porous wall where the temperature of the solid phase is important. The temperature of volume element i is governed by eq. (4), which considers the net heat inflow into volume element i due to convection $Q_{\text{conv},i}$, conduction $Q_{\text{cond},i}$, advection $Q_{\text{flow},i}$ and reaction $Q_{\text{react},i}$:

$$C_i \frac{\mathrm{d}T_i}{\mathrm{d}t} = Q_{\text{conv},i} + Q_{\text{cond},i} + Q_{\text{flow},i} + Q_{\text{react},i}, \tag{4}$$

where the heat capacity of the volume element is denoted as C_i. The convective heat transfer between volume element i and j is controlled by the heat transfer coefficient $h_{\text{conv},ij}$,the heat transfer area $A_{\text{conv},ij}$ and the temperature difference between the volume elements $(T_j - T_i)$:

$$Q_{\text{conv},i} = \sum_{\forall j} h_{\text{conv},ij} A_{\text{conv},ij} \left(T_j - T_i\right). \tag{5}$$

The heat of conduction between volume element i and j is calculated according to eq. (6), a linearised version of the heat diffusion equation. It depends on the thermal conductivity of the solid phase λ and the length between the volume elements $L_{\text{cond},ij}$:

$$Q_{\text{cond},i} = \sum_{\forall j} \frac{\lambda V_i}{L^2_{\text{cond},ij}} \left(T_j - T_i\right). \tag{6}$$

The contribution to the energy balance due to gas flow is governed by:

$$\begin{aligned} Q_{\text{flow},i} = &\sum_{\forall \text{in}} \dot{m}_{\text{in}} \sum_{\forall \gamma} Y_{\gamma,\text{in}} \left(\hat{H}_{\gamma,\text{in}} - \hat{H}_{\gamma,i}\right) \\ &+ \sum_{\forall \text{in}} \dot{m}_{\text{in}} \sum_{\forall \gamma} \frac{RT_i}{M_\gamma} \left(Y_{\gamma,\text{in}} - Y_{\gamma,i}\right), \end{aligned} \tag{7}$$

where $\hat{H}_\gamma$ is the mass-specific enthalpy of gas species γ. The heat due to chemical reactions is calculated:

$$Q_{\text{react},i} = V_i \sum_{\forall \gamma} \hat{U}_{\gamma,i} M_\gamma \sum_{\forall w} \nu_{\gamma,w} r_{w,i}, \tag{8}$$

where $\hat{U}_\gamma$ is the mass-specific internal energy of gas species γ.
The particle mass distributions in the system are described by a sectional method, with each section describing the number of particles with a given range of masses. The particles are assumed to be spherical and purely carbonaceous. Particles in the gas phase in the channels are considered to be freely suspended, and the evolution of the population in each volume element is solved analogously to eq. (3). On the other hand, particles inside the cake layer and the porous wall are considered immobile. The number density of trapped particles N in size class η is governed by filtration and regeneration as shown in eq. (9):

$$\frac{\mathrm{d}N_{\eta,i}}{\mathrm{d}t} = \theta_{\eta,i} \dot{N}_{\eta,\text{in}} + k\left[\mathrm{O_2}\right] \left(\pi d^2_{\text{p},\eta} N_{\eta,i}\right), \tag{9}$$

where θ_η is the size-specific filtration efficiency, $\dot{N}_{\eta,\text{in}}$ is the inflow of number density of particles in size class η, k is the rate constant, $[\mathrm{O_2}]$ is the oxygen concentration and $d_{\text{p},\eta}$ is the particle diameter of size class η. The expression of rate constant is from an accepted model from the literature [15]. The value of activation energy in the rate constant k is taken as 150 kJ/mol [16]. The pre-exponential factor in the rate constant was calibrated based on the outlet temperature of the DPF observed by Rothe et al. [23]. It was left unchanged for the remainder of the work. The chemical equation of active regeneration is from the same study:

$$\mathrm{C} + \alpha \mathrm{O_2} \rightarrow (2\alpha - 1)\,\mathrm{CO_2} + (2 - 2\alpha)\,\mathrm{CO}, \tag{10}$$

where α is the stoichiometric parameter for the regeneration reaction. The stoichiometric parameter for the oxidation reaction was calculated from the CO-to-CO_2 ratio measured by Rothe et al. [23] using Thermo-Gravimetric Analysis (TGA).

2.2 Unit collector model

The unit collector model is widely used to model the filtration performance of DPFs [26]. The model describes the pore space in the porous wall of a monolith as spherical unit collectors with the same porosity as the wall. The flow in the porous wall is considered by an equivalent flow around the spherical core of the collector, which represents the wall substrate as shown in Fig. 2.

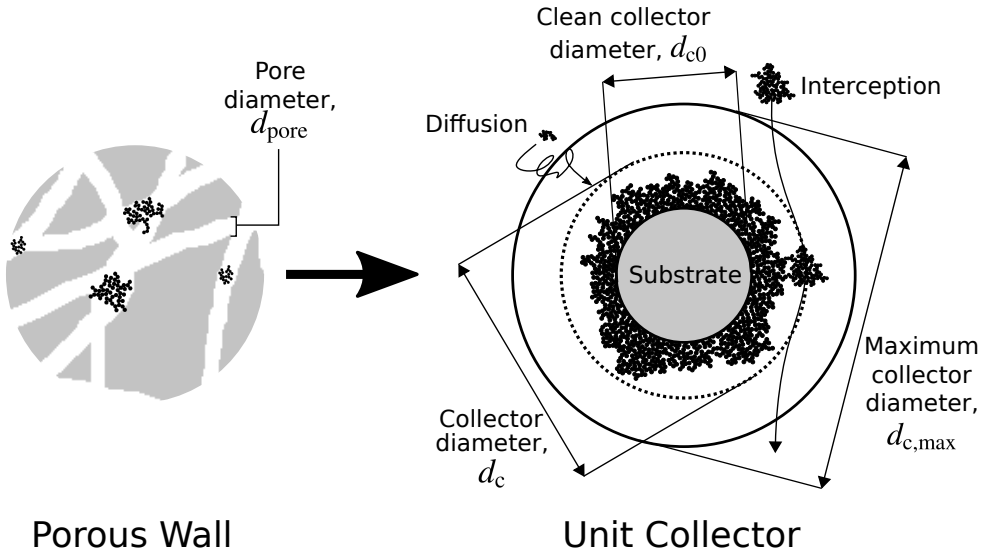

Figure 2: *Schematic unit collector model. Particle filtration in the porous wall is modelled as particle flow around the spherical collector. The effective diameter of the collector grows as particles are trapped.*

The collector diameter of the clean DPF d_{c0} is defined as a function of the clean wall porosity ε_0 and the pore diameter d_{pore}:

$$d_{c0} = \frac{3}{2}\frac{1-\varepsilon_0}{\varepsilon_0} d_{pore}. \tag{11}$$

Whilst the wall porosity and the pore diameter can be measured experimentally, they were not reported by Rothe et al. [23]. In this study, the clean wall porosity was calibrated to be 0.5 based on experimental observations of the thermal mass of the DPF studied by Rothe et al. [23] . This value is within the range found in literature [3]. The pore diameter was calibrated based on experimentally observed filtration efficiency during loading.

Two collection mechanisms are considered in the unit collector model. Particles can be trapped either when they diffuse towards the core due to Brownian motion or when they intercept the core whilst flowing around it. These two mechanisms model the deep-bed

filtration process inside the porous wall. Filtration due to inertial impaction has a minor effect only in the context of engine exhaust and is neglected in the current model [11].

The collector diameter d_c grows as particles are trapped in the model. The filtration efficiency of the porous particle cake layer itself is not considered explicitly by the unit collector model; rather it is derived from the state of the porous wall. A partition coefficient is defined to capture the transition from deep-bed filtration to cake formation. The partition coefficient in the original unit collector model Φ_{UC} is a function of a model parameter, the *percolation constant* ψ, the diameter of collector at the interface between the porous wall and the cake $d_{c,interface}$ and the maximum allowed collector diameter $d_{c,max}$:

$$\Phi_{UC} = \frac{d_{c,interface}^2 - d_{c0}^2}{(\psi d_{c,max})^2 - d_{c0}^2}. \tag{12}$$

The contribution of the wall to the pressure drop is a function of the wall thickness and the wall permeability in the model. The impact of pore blocking on the pressure drop is captured in the model by the change in the permeability as the wall is loaded with particles. The pressure drop due to the cake is calculated based on its thickness, assuming constant cake porosity. The permeability of the cake is a function of its porosity and the diameter of particles in the cake. The detailed model equations can be found in the literature [18, 19, 26].

2.3 Extended model

It was observed in the experiments by Rothe et al. [23] that the filtration efficiency of the DPF decreased during active regeneration. As it is shown later in Section 4.1, the original unit collector model, which considers only the removal of the cake layer and wall-trapped particles, cannot describe the experimental measurements satisfactorily. Further, the filtration efficiency predicted by the original model at regenerating condition actually *increases* due to increased Brownian motion at high temperature.
The unit collector model is therefore modified in order to improve the model performance. This study focuses on solid particulate emissions since measurements of semi-volatile particles are less reliable due to high sensitivity to the sampling condition. The literature suggests that soot fragmentation only occurs in catalytic DPFs [6]. As a result, fragmentation is not considered here since the DPF studied by Rothe et al. [23] has no catalytic coating. Thermal pore expansion and hysteretic cake filtration sub-models are added to the unit collector model and are described in the sections below.

2.3.1 Pore expansion

It was suggested by Rothe et al. [23] that thermal expansion of the porous wall may be a possible explanation for the observed decrease in filtration efficiency during regeneration. The clean filtration efficiency predicted by the unit collector model is controlled by the thickness, porosity and the pore diameter of the porous wall. Based on the thermal expansion coefficient of SiC [3], the volumetric strain of the porous wall during regeneration is

estimated to be 0.16%. It is expected that the change in the wall thickness and the wall porosity will be of the same order of magnitude. It was observed during model calibration that the model performance was insensitive to the variation in the wall porosity and the wall thickness if their changes were within 1%. They were therefore treated as constant in this study.

The pore diameter, on the other hand, may be more affected. The microstructure of a porous medium consists of complex networks of channels. The pore size distribution in the wall can cover a wide range of sizes (e.g. 1–20 microns [7]). Whilst the model could be modified to consider a distribution of pore sizes [11], it would not be practical to do this in this particular study due to the lack of information about the wall structure of the DPF used in the experiment. The pore diameter in the wall is a calibrated parameter in the unit collector model; it is a length scale that parameterises the filtration ability of the pore structure in the filter wall. In order to investigate whether a change in the modelled pore diameter is able to explain the experimentally observed decrease in filtration efficiency, the pore diameter of the filter wall is modelled as having a linear dependence on the local wall temperature in this study,

$$d_{\text{pore}} = \beta \left(T - T_{\text{ref}}\right) + d_{\text{pore,ref}}, \tag{13}$$

where $d_{\text{pore,ref}}$ is the pore diameter at the reference temperature T_{ref} (in this case, 320 °C, the inlet temperature of the DPF before regeneration). The pore expansion constant β is calibrated based on the experimental filtration efficiency of the DPF during active regeneration in this study.

2.3.2 Hysteretic cake

Equation (12) describes the filtration efficiency of the cake as a function of the state of the wall, but independent of the cake itself. This form of equation is not suitable to describe regeneration. Typically the amount of material trapped inside the wall is an order of magnitude lower than that in the cake. Given sufficient oxidant supply, the wall can be regenerated completely whilst significant material remains in the cake [7]. Eq. (12) will erroneously predict a zero-value partition coefficient under this situation, such that incoming particles would "bypass" the cake entirely. It is apparent that the filtration efficiency of cake should also depend on the state of the cake.

The evolution of the cake during regeneration was studied by Choi et al. [7]. The cake profile during a loading-regenerating cycle is shown schematically in Fig. S1. It was found that the deposits directly above the open pores of the wall were oxidised more rapidly than those deposited on the wall substrate. Owing to the existence of these open pores, the cake is no longer an effective barrier to incoming particles despite significant material remain on the wall surface. Based on these observations, the following empirical logistic function is proposed to describe the partition coefficient of the cake during regeneration

Φ_{regen}:

$$\Phi_{\text{regen}} = \frac{\exp\left[\omega_1\left(\frac{m_{\text{p}}}{m_{\text{p0}}} - \omega_2\right)\right]}{\exp\left[\omega_1\left(\frac{m_{\text{p}}}{m_{\text{p0}}} - \omega_2\right)\right] + 1}, \tag{14}$$

where the mass of trapped particles in the cake is denoted as m_{p}. The initial cake mass is denoted as m_{p0}. Two numerical parameters, ω_1 and ω_2, were calibrated based on the experimental filtration efficiency of the DPF during active regeneration in this study. The filtration efficiency of the cake will decrease rapidly when the dimensionless cake mass drops below ω_2.

Note that this mechanism is in addition to the original partition coefficient since the nominal filtration efficiency of the cake will be 100% when the porous wall is fully loaded. Assuming that the two mechanisms are independent, the overall partition coefficient Φ_{overall} is:

$$\Phi_{\text{overall}} = \Phi_{\text{UC}} + \Phi_{\text{regen}} - \Phi_{\text{UC}}\Phi_{\text{regen}}, \tag{15}$$

which is derived assuming that the partition coefficients are dimensionless probabilities.

3 Experimental setup

The experimental setup used by Rothe et al. [23] is summarised. A 10.5 L Euro-IV compliant heavy duty diesel engine was studied. A Diesel Oxidation Catalyst (DOC) and a DPF were installed downstream of the engine. The cordierite DOC was coated with platinum and palladium. The DPF was made of SiC without any catalytic coating. A fuel injection system with autonomous control was installed between the engine and the DOC. Fuel was able to be injected into the exhaust, such that it oxidised in the DOC, causing active regeneration in the DPF due to the heat released from the oxidation in the DOC. The experimental setup is shown in Fig. S2.

Prior to active regeneration, the DPF was loaded with particulates to approximately 3 g/L by running the engine with a low-load drive cycle for 20 h. The mass flow rate of particulates was 3.6 g/h. After the particle loading phase, active regeneration experiments were carried out for 20 min, where the engine operated at steady condition. The regeneration experiment was repeated after the DPF was completely regenerated, but this study will focus on the first part of the experiment where a loaded DPF was regenerated.
The temperature and pressure at the inlet of DOC, the inlet of DPF and the outlet of DPF were measured. The gas phase compositions before and after the after-treatment system were measured but the composition at the inlet of the DPF was not reported. The inlet oxygen mole fraction was assumed to be 10% in this study based on results from similar experiments [1]. It was observed that this assumption had no significant impact on the model performance. Similar performance could be achieved for inlet oxygen mole fractions between 5% and 15%.
The particulate emissions at the outlet were measured by four devices: An Advanced

Particle Counter (APC) which was PMP compliant and reported the solid PN; an Engine Exhaust Particle Sizer (EEPS) which reported the combined particle size distribution of solid and semi-volatile particles; a Micro Soot Sensor (MSS) which reported the PM; and the Filter Smoke Number (FSN). Based on the APC and EEPS measurements, it was concluded by Rothe et al. [23] that semi-volatile particle emissions were negligible for the system and conditions studied in the experiment. This is supported by the TGA data that show limited mass loss ($\leq$ 2%) from soot samples at low temperature ($\leq$ 300°C). Therefore only measurements made by APC and MSS were used for model calibration. For this reason, the current study is limited to solid particles only. Furthermore, it was observed that the mode diameter of outlet particles was 80 nm. The absence of smaller particles suggested that soot fragmentation did not occur. Semi-volatile particle nucleation and soot fragmentation are therefore neglected in this study.
The PM and PN filtration efficiencies based on raw exhaust measurements were reported. However, the particle size distribution at the inlet of the DPF was not measured. For this reason, the inlet particle size distribution is assumed to be a single-mode log-normal distribution [14]. It was shown during calibration that the phenomenological conclusions of this study are not sensitive to this assumption.
Full details of the model calibration procedure are shown in Fig. S3. The calibration procedure follows three steps. Firstly, the model is calibrated to match the behaviour of the clean DPF. Secondly, the model is calibrated to capture the filtration behaviour of the DPF during particle loading. Finally, the model is calibrated against the active regeneration data.

4 Results and discussion

4.1 Original unit collector model

The particle loading experiment was first simulated using the original unit collector model. The parameters of the unit collector model were calibrated to match the pressure drop, PM and PN efficiencies during the loading of the filter, and were left unchanged for the remainder of this work. The values of the model input are shown in Table S1. Good agreement between the model predictions and experimental measurements of the pressure drop and filtration efficiency during loading are seen in Fig. 3.

The model was then applied to simulate the active regeneration experiment. The predicted temperature profile is shown in Fig. 4. There is acceptable agreement during the heat up of the DPF until a maximum temperature is reached. However, the model does not capture an unexpected event where the outlet temperature drops below that of the inlet. The experimental outlet temperature is observed to decrease between 400 and 700 s, eventually falling below the inlet temperature. No explanation was provided with the measurements. Additional figures showing the DPF wall temperature and the pressure drop across the system during regeneration are shown in Figs. S4 and S5 respectively.

The original unit collector model predicts that only 0.2% of the inlet particles pass through the DPF at the end of regeneration, whereas the experimentally observed value was approximately 2.5%. It is clear that the removal of particles from the cake layer and from

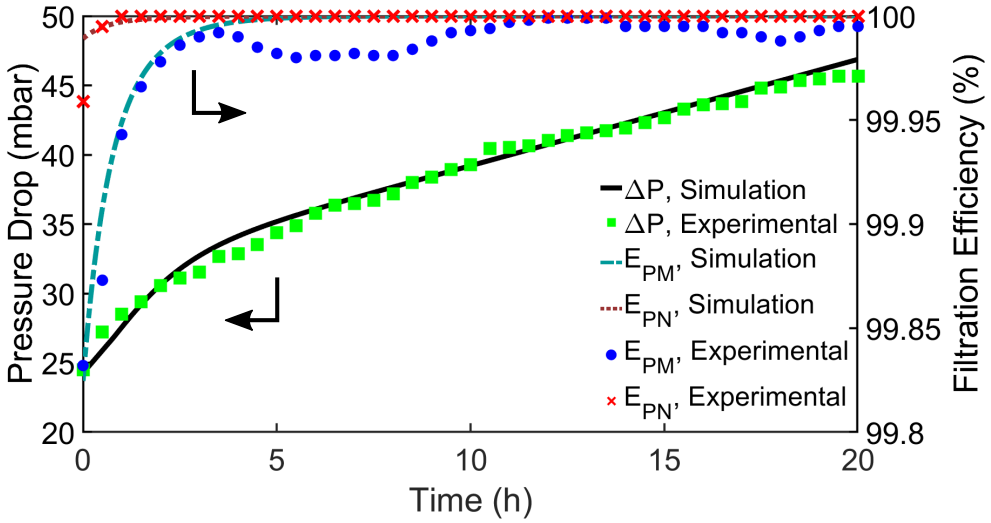

Figure 3: *Pressure drop and filtration efficiency of DPF during loading.*

inside the porous walls is insufficient to explain the experimentally observed decrease in the filtration efficiency. It is considered highly unlikely that particles introduced by oxidation of the fuel injected into the DOC are responsible for this difference because the required mass of the extra particle inflow would be an order of magnitude higher than the engine-out particle mass flow. This motivates the decision to extend the unit collector model.

4.2 Extended unit collector model

Two versions of extended model were used to simulate the active regeneration experiment: One with the abbreviation "P.E." considers the thermal pore expansion described by eq. (13), the other with the abbreviation "P.E.+M.C." considers both pore expansion and the cake filtration sub-model described by eq. (15). The PM and PN filtration efficiencies are shown in Fig. 5. The modelled filtration efficiency decreases during regeneration. The decrease was more significant for larger particles (100 nm) than smaller particles (30 nm). This is consistent with the experimental observations that larger particles rather than smaller particles are emitted during regeneration.

The agreements between the final predicted filtration efficiencies and final experimental filtration efficiencies are improved by considering thermal pore expansion. The calibrated pore diameter at the end of regeneration is 23.2 μm (600 °C) in contrast to 13.1 μm before regeneration (320 °C). However, considering pore expansion alone did not yield agreement with the rapid rate of change of filtration efficiency at breakthrough. Satisfactory agreement was only obtained when the cake filtration sub-model was also included. The inclusion of thermal pore expansion and cake filtration was necessary to reproduce the experimentally observed rapid rate of change and the decrease in the final filtration efficiency. At this stage, neither version of the extended model is able to capture the transient drop in filtration efficiency at around 500 s. It is noted that this corresponds to the period of negative temperature gradient in Fig. 4. The cause of both effects remains an

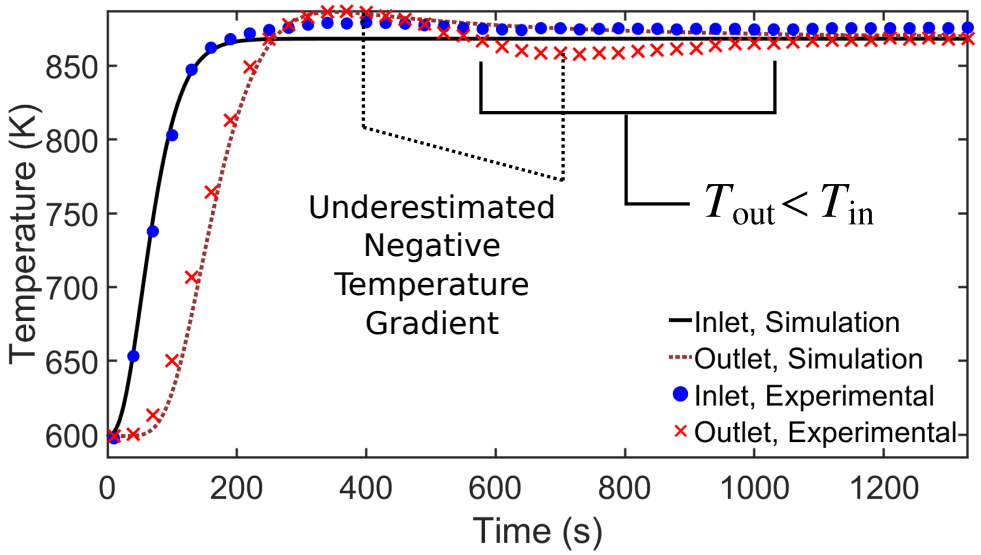

Figure 4: *DPF temperature profiles during regeneration.*

area of investigation.

5 Conclusion

In this study, the unit collector filtration model is coupled to a population balance model to describe an experimentally studied DPF undergoing active regeneration. The original unit collector model was shown to overestimate the filtration efficiency of the DPF during active regeneration. The model was extended to include thermal pore expansion in the wall as well as non-uniform dissolution of the particle cake layer. These extensions allow better prediction of the final filtration efficiency of the DPF and the timing when the filtration efficiency begins to decrease. The phenomenological advantages of the extended model were clearly shown and were independent of the assumed inlet particle size distribution. The model improves our understanding of the sources of particulate emissions during the regeneration of diesel particulate filters. In particular, the study has shown that the filtration efficiency of the particle cake layer should be considered in its own right, rather than being derived from the state of the porous wall. It should be noted that this study is limited to solid particle emission only. In the future, the model should be tested against other sets of experimental data [for example 6, 17, 27] to evaluate the capability of the current formulation. Further investigation will be required to better understand the transient behaviour of active regenerating DPFs and to extend the model to consider the fibrous nature of the soot cake layer. Finally, the authors would like to stress the importance of reporting experimental data for both the inlet and the outlet particle size distributions to support the development of this type of model.

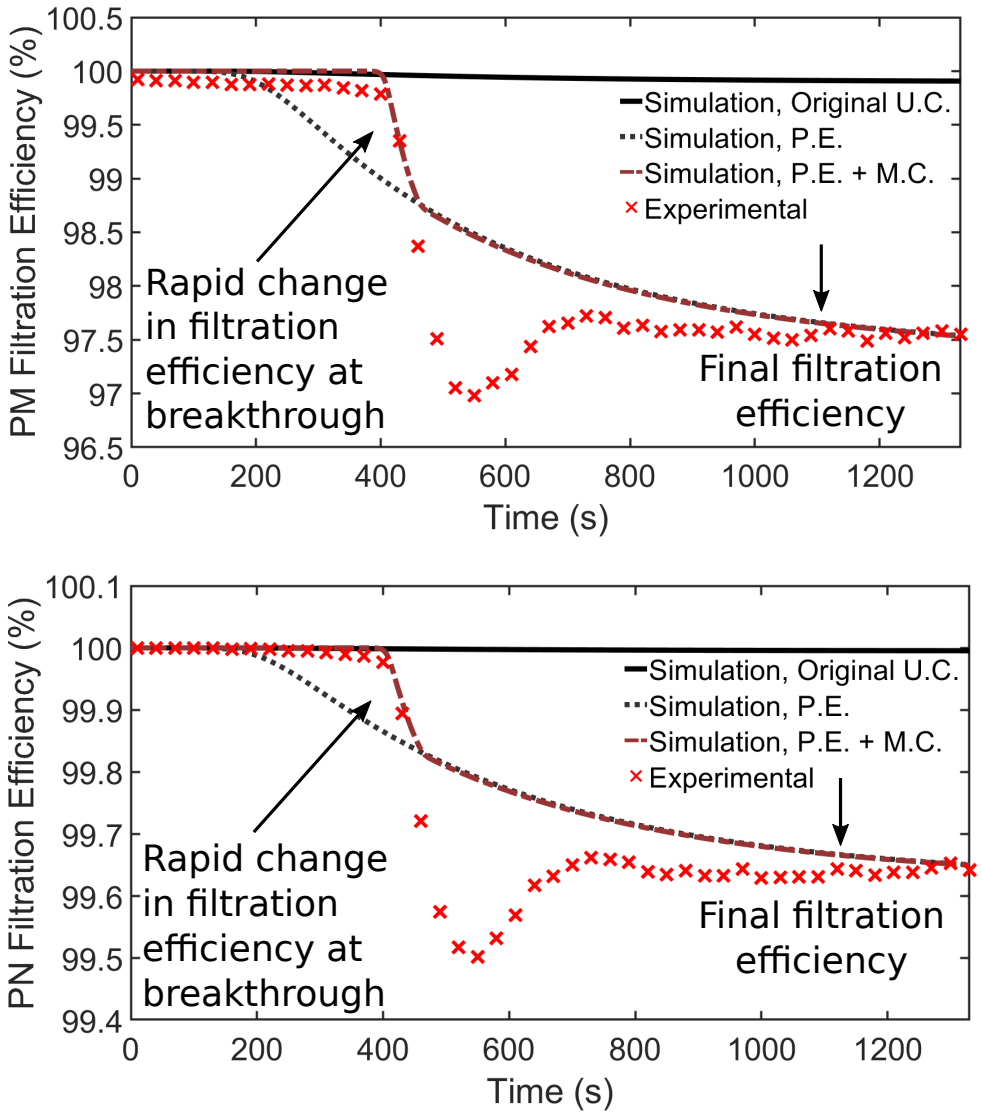

Figure 5: *Simulated filtration efficiencies of DPF during regeneration.*

Supplementary material

Additional data related to this publication is available at the University of Cambridge data repository (https://doi.org/10.17863/CAM.26023).

Acknowledgements

The authors would like to thank Cambridge Centre for Advanced Research and Education in Singapore (CARES), Engineering and Physical Sciences Research Council (EPSRC) and Royal Dutch Shell for their support. This project has received funding from the European Union's Horizon 2020 Research and Innovation Programme under grant agreement no. 724145.

References

[1] C. Beatrice, S. D. Iorio, C. Guido, and P. Napolitano. Detailed characterization of particulate emissions of an automotive catalyzed DPF using actual regeneration strategies. *Experimental Thermal and Fluid Science*, 39:45–53, 2012. ISSN 08941777. doi:10.1016/j.expthermflusci.2012.01.005.

[2] C. Beatrice, M. A. Costagliola, C. Guido, P. Napolitano, and M. V. Prati. How much regeneration events influence particle emissions of dpf-equipped vehicles? In *13th International Conference on Engines & Vehicles*. SAE International, sep 2017. doi:https://doi.org/10.4271/2017-24-0144.

[3] C. Benaqqa, M. Gomina, A. Beurotte, M. Boussuge, B. Delattre, K. Pajot, E. Pawlak, and F. Rodrigues. Morphology, physical, thermal and mechanical properties of the constitutive materials of diesel particulate filters. *Applied Thermal Engineering*, 62 (2):599–606, 2014. ISSN 13594311. doi:10.1016/j.applthermaleng.2013.10.024.

[4] S. Bensaid, D. D. L. Marchisio, D. Fino, G. Saracco, and V. Specchia. Modelling of diesel particulate filtration in wall-flow traps. *Chemical Engineering Journal*, 154 (1-3):211–218, nov 2009. ISSN 13858947. doi:10.1016/j.cej.2009.03.043.

[5] S. Bensaid, C. J. Caroca, N. Russo, and D. Fino. Detailed investigation of non-catalytic DPF regeneration. *Canadian Journal of Chemical Engineering*, 89(2):401–407, 2011. ISSN 00084034. doi:10.1002/cjce.20408.

[6] E. Cauda, S. Hernandez, and D. Fino. PM 0.1 emissions during diesel trap regeneration. *Enviormental science & technology*, 40(17):5532–5537, 2006.

[7] S. Choi, K.-C. Oh, and C.-B. Lee. The effects of filter porosity and flow conditions on soot deposition/oxidation and pressure drop in particulate filters. *Energy*, 77: 327–337, 2014. ISSN 03605442. doi:10.1016/j.energy.2014.08.049.

[8] C. Depcik and D. Assanis. Simulating Area Conservation and the Gas-Wall Interface for One-Dimensional Based Diesel Particulate Filter Models. *Journal of Engineering for Gas Turbines and Power*, 130(6):062807–1–062807–18, 2008. ISSN 07424795. doi:10.1115/1.3155792.

[9] J. E, L. Xie, Q. Zuo, and G. Zhang. Effect analysis on regeneration speed of continuous regeneration-diesel particulate filter based on NO_2-assisted regeneration. *Atmospheric Pollution Research*, 7(1):9–17, 2016. ISSN 13091042. doi:10.1016/j.apr.2015.06.012.

[10] N. M. Ghoniem. High-temperature mechanical and material design for SiC composites. *Journal of Nuclear Materials*, 191-194:515–519, 1992. ISSN 00223115. doi:10.1016/S0022-3115(09)80098-6.

[11] J. Gong and C. J. Rutland. PDF-based heterogeneous multiscale filtration model. *Environmental Science and Technology*, 49(8):4963–4970, 2015. ISSN 15205851. doi:10.1021/acs.est.5b00329.

[12] B. Guan, R. Zhan, H. Lin, and Z. Huang. Review of the state-of-the-art of exhaust particulate filter technology in internal combustion engines. *Journal of Environmental Management*, 154:225–258, 2015. ISSN 03014797. doi:10.1016/j.jenvman.2015.02.027.

[13] O. A. Haralampous and G. C. Koltsakis. Oxygen diffusion modeling in diesel particulate filter regeneration. *AIChE Journal*, 50(9):2008–2019, 2004. ISSN 00011541. doi:10.1002/aic.10181.

[14] S. J. Harris and M. Maricq. Signature size distributions for diesel and gasoline engine exhaust particulate matter. *Journal of Aerosol Science*, 32(6):749–764, jun 2001. ISSN 00218502. doi:10.1016/S0021-8502(00)00111-7.

[15] I. P. Kandylas and G. C. Koltsakis. NO_2-Assisted Regeneration of Diesel Particulate Filters: A Modeling Study. *Industrial & Engineering Chemistry Research*, 41(9): 2115–2123, 2002. ISSN 0888-5885. doi:10.1021/ie010842m.

[16] E. A. Kladopoulou, S. L. Yang, J. H. Johnson, G. G. Parker, and A. G. Konstandopoulos. A study describing the performance of diesel particulate filters during loading and regeneration - a lumped parameter model for control applications. In *SAE 2003 World Congress & Exhibition*. SAE International, mar 2003. doi:https://doi.org/10.4271/2003-01-0842.

[17] J. Ko, W. Si, D. Jin, C.-L. Myung, and S. Park. Effect of active regeneration on time-resolved characteristics of gaseous emissions and size-resolved particle emissions from light-duty diesel engine. *Journal of Aerosol Science*, 91:62–77, 2016. ISSN 00218502. doi:10.1016/j.jaerosci.2015.09.007.

[18] A. G. Konstandopoulos, M. Kostoglou, E. Skaperdas, E. Papaioannou, D. Zarvalis, and E. Kladopoulou. Fundamental studies of diesel particulate filters: Transient loading, regeneration and aging. In *SAE 2000 World Congress*. SAE International, mar 2000. doi:https://doi.org/10.4271/2000-01-1016.

[19] A. G. Konstandopoulos, E. Skaperdas, and M. Masoudi. Microstructural properties of soot deposits in diesel particulate traps. In *SAE 2002 World Congress & Exhibition*. SAE International, mar 2002. doi:https://doi.org/10.4271/2002-01-1015.

[20] J. Lelieveld, J. S. Evans, M. Fnais, D. Giannadaki, and A. Pozzer. The contribution of outdoor air pollution sources to premature mortality on a global scale. *Nature*, 525(7569):367–371, 2015. ISSN 0028-0836. doi:10.1038/nature15371.

[21] K. Ramanathan, V. Balakotaiah, and D. H. West. Light-off criterion and transient analysis of catalytic monoliths. *Chemical Engineering Science*, 58(8):1381–1405, 2003. ISSN 00092509. doi:10.1016/S0009-2509(02)00679-6.

[22] V. Ramanathan and G. Carmichael. Global and regional climate changes due to black carbon. *Nature Geoscience*, 1(4):221 – 227, 2008. ISSN 1752-0894. doi:10.1038/ngeo156.

[23] D. Rothe, M. Knauer, G. Emmerling, D. Deyerling, and R. Niessner. Emissions during active regeneration of a diesel particulate filter on a heavy duty diesel engine: Stationary tests. *Journal of Aerosol Science*, 90:14–25, 2015. ISSN 18791964. doi:10.1016/j.jaerosci.2015.07.007.

[24] L. Sileghem, D. Bosteels, J. May, C. Favre, and S. Verhelst. Analysis of vehicle emission measurements on the new WLTC, the NEDC and the CADC. *Transportation Research Part D: Transport and Environment*, 32:70–85, oct 2014. ISSN 13619209. doi:10.1016/j.trd.2014.07.008.

[25] K. Yamamoto and Y. Kanamori. Measurements of size distribution and oxidation rate of pm with no_2. In *JSAE/SAE 2015 International Powertrains, Fuels & Lubricants Meeting*. SAE International, sep 2015. doi:https://doi.org/10.4271/2015-01-1995.

[26] S. Yang, C. Deng, Y. Gao, and Y. He. Diesel particulate filter design simulation: A review. *Advances in Mechanical Engineering*, 8(3):1–14, 2016. ISSN 1687-8140. doi:10.1177/1687814016637328.

[27] S. Yoon, D. C. Quiros, H. A. Dwyer, J. F. Collins, M. Burnitzki, D. Chernich, and J. D. Herner. Characteristics of particle number and mass emissions during heavy-duty diesel truck parked active DPF regeneration in an ambient air dilution tunnel. *Atmospheric Environment*, 122:58–64, dec 2015. ISSN 13522310. doi:10.1016/j.atmosenv.2015.09.032.

[28] M. Yu, D. Luss, and V. Balakotaiah. Regeneration modes and peak temperatures in a diesel particulate filter. *Chemical Engineering Journal*, 232:541–554, oct 2013. ISSN 13858947. doi:10.1016/j.cej.2013.08.006.

Appendix

Table S1: *Model input.*

Parameter	Symbol	Value	Unit	Ref.
Inlet gas mass flow	$\dot{m}_{\text{in}}$	586	kg/h	-
Particle mass flow	-	3.6	g/h	[23]
Inlet particle geometric mean diameter	-	38	nm	-
Inlet particle standard deviation	-	1.48	-	-
Inlet Oxygen mole fraction	$[O_2]_{\text{in}}$	10	%	[1]
DPF length	-	304.8	mm	[23]
DPF diameter	-	304.8	mm	[23]
DPF cell density	-	200	cpsi	[23]
DPF wall thickness	L_{pw}	0.381	mm	-
DPF wall permeability	κ	1.22×10^{-13}	m^2	-
DPF wall porosity	ε_0	50	%	-
DPF wall pore diameter (320°C)	$d_{\text{pore,ref}}$	13.1	μm	-
Soot packing density in wall	-	16	kg/m^3	-
Percolation constant	ψ	0.87	-	-
Soot cake porosity	-	0.94	-	-
Soot cake primary particle diameter	-	15	nm	-
DPF heat capacity	C_{DPF}	15942	J/K	[10]
DPF thermal conductivity	λ	90	W/mK	[3]
DPF channel heat transfer coefficient	h_{conv}	129.3	W/m^2K	[21]
Axial discretisation	-	10	-	-
Wall discretisation	-	5	-	-
Regeneration rate pre-exponential factor	-	1.5×10^{24}	m/molKs	-
Regeneration activation energy	-	150	kJ/mol	[16]
Regeneration stoichiometric parameter	α	0.83	-	-
Pore expansion gradient	β	3.7×10^{-8}	m/K	-
Pore expansion reference temperature	T_{ref}	320	°C	[23]
Initial cake mass	m_{p0}	0.0679	kg	-
Soot cake filtration parameter 1	ω_1	150.0	-	-
Soot cake filtration parameter 2	ω_2	0.546	-	-

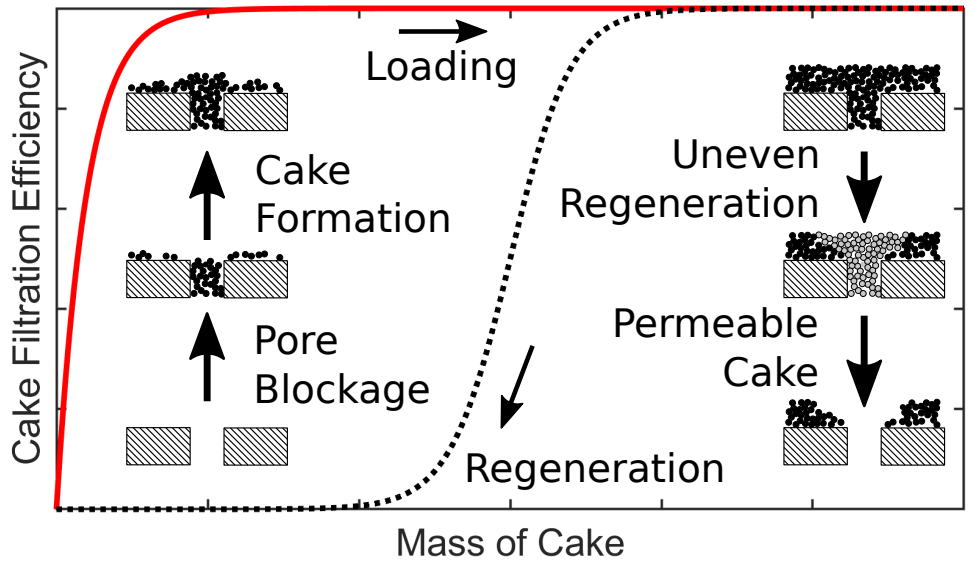

Figure S1: *The filtration efficiency of the cake should exhibit a hysteretic behaviour during a load-regeneration cycle. The cake is no longer uniform during regeneration. Holes in the cake lead to decreased filtration efficiency despite significant cake mass remaining on the substrate of the wall.*

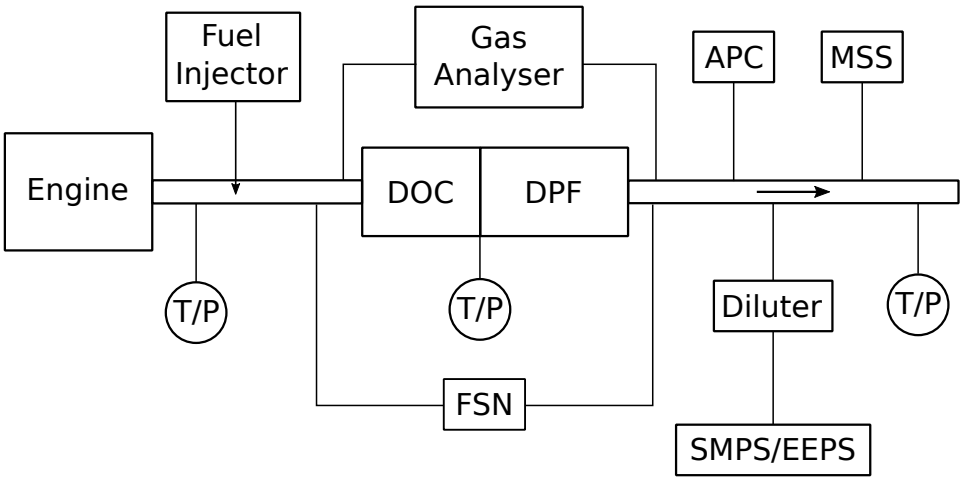

Figure S2: *Experimental setup used by [23]. "T/P" indicates temperature and pressure measurements.*

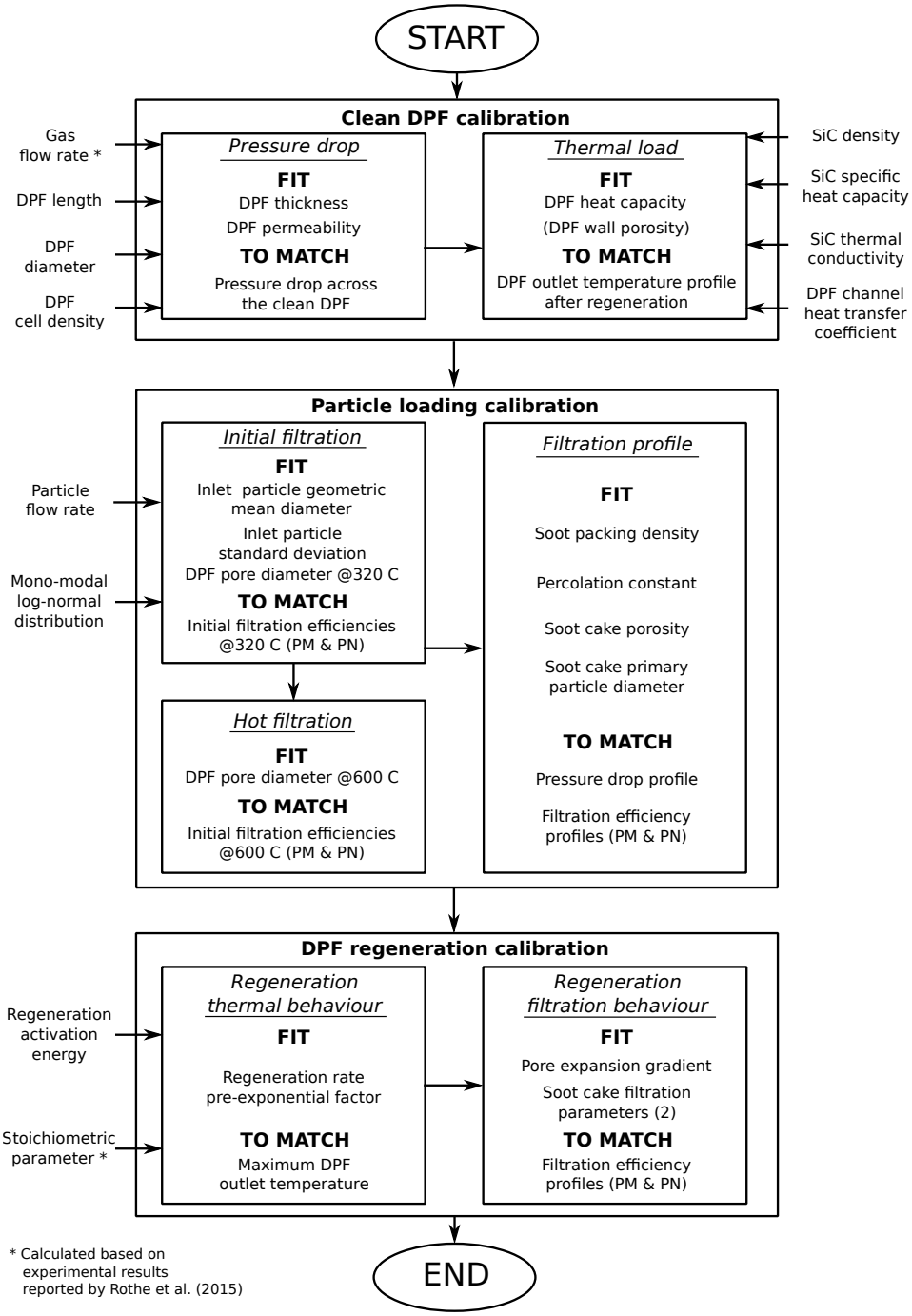

Figure S3: *Block diagram for the calibration procedures. Once calibrated, the values of parameters are fixed for all subsequent parts of the calibration procedure and all subsequent use of the model.*

Clean DPF calibration

Pressure drop

The length, diameter and cell density of the DPF are reported by Rothe et al. [23]. The gas flow-rate is calculated from the CO concentration, specific CO emissions, engine speed and torque reported by Rothe et al. [23].

The thickness and the permeability of the wall of DPF are calibrated to match the pressure drop over the clean DPF reported by Rothe et al. [23]. Since this problem is under-specified (calibrating two input variables to match one output variable), the resulting thickness and permeability are not unique. Their values are chosen such that they lie in typical ranges based on literature review [4, 9]. Ideally, the thickness of wall would be measured. However this data was not available, so the wall thickness was included in the calibration procedure in this case. The calibration of the permeability is consistent with the standard calibration procedure for the original unit collector model [16, 18].

Thermal load

The thermal conductivity [3], specific heat capacity and density [10] of silicon carbide (SiC) are taken from the literature. The convective heat transfer coefficient between channel flow and the porous wall is calculated using the gas flow rate and correlation from Ramanathan et al. [21].

The overall heat capacity of the DPF is calibrated to match the DPF outlet temperature profile after regeneratiion has completed (where the DPF is clean). The porosity of the wall of the DPF is then calculated from the calibrated overall heat capacity using the specific heat capacity and the density of SiC.

Particle loading calibration

Initial filtration

The particle flow rate is reported by Rothe et al. [23]. The inlet particle size distribution was not reported, and is therefore assumed to be a mono-modal log-normal distribution, characterised by a geometric mean diameter and geometric standard deviation.

The modelled filtration efficiency of the clean DPF is governed by the thickness, porosity and pore diameter of the porous wall. It is assumed that the change in filtration efficiency is due a change in the local pore diameter caused by the change in the local wall temperature during regeneration. The geometric mean diameter and the standard deviation of the inlet particle size distribution (in the absence of experimental data) and the pore diameter of the porous wall at 320°C were calibrated to match the experimental measured mass- and number-based filtration efficiency at the beginning of particle loading experiment.

This is consistent with the standard calibration procedure for the original unit collector model [16].

Hot filtration

The pore diameter of the porous wall at 600°C was calibrated (without changing the inlet particle distribution) to match the experimental measured mass- and number-based filtration efficiency at the end of active regeneration (when the DPF is clean).

Filtration profile (Fig. 3)

The soot packing density, percolation constant, soot cake porosity and soot cake primary particle diameter are calibrated to match the measured pressure drop profile and filtration efficiencies profiles (mass- and number-based) during the particle loading experiment. All four parameters affect the rate of pressure drop increase during transition between deep bed filtration and cake formation stage; the pressure drop profile during cake formation stage is controlled by soot cake porosity and soot cake primary particle diameter. This is consistent with the standard calibration procedure for the original unit collector model [16, 18, 19].

DPF regeneration calibration

Regeneration thermal behaviour (Fig. 4)

The activation energy of the regeneration reaction is obtained from literature [16]. The stoichiometric parameter of the oxidation reaction is calculated from the ratio of CO and CO_2 produced from particles during TGA experiment performed by Rothe et al. [23].

The pre-exponential factor of regeneration reaction is calibrated to match the DPF outlet temperature profile during regeneration. In particular, it is noted that the pre-exponential factor has a strong influence on the value and the timing of maximum DPF outlet temperature.

Regeneration filtration behaviour (Fig. 5)

The pore expansion gradient (β) and the two soot cake filtration parameters (ω_1 , ω_2), as described in eq. (13) and (14) respectively, are calibrated to match the mass- and number-based filtration efficiencies of the DPF during active regeneration.

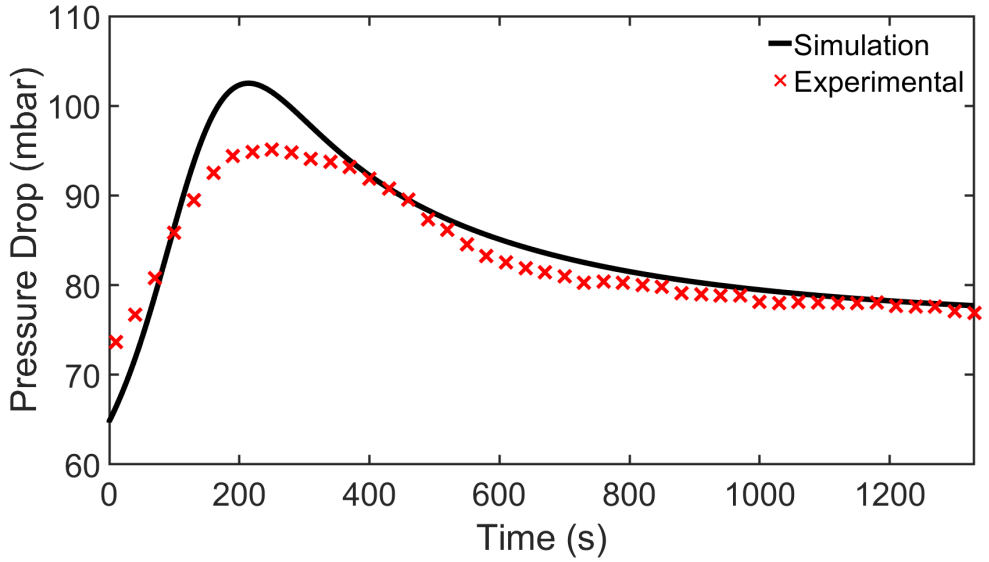

Figure S4: *Comparison between experimentally measured and simulated pressure drop across the system during regeneration.*

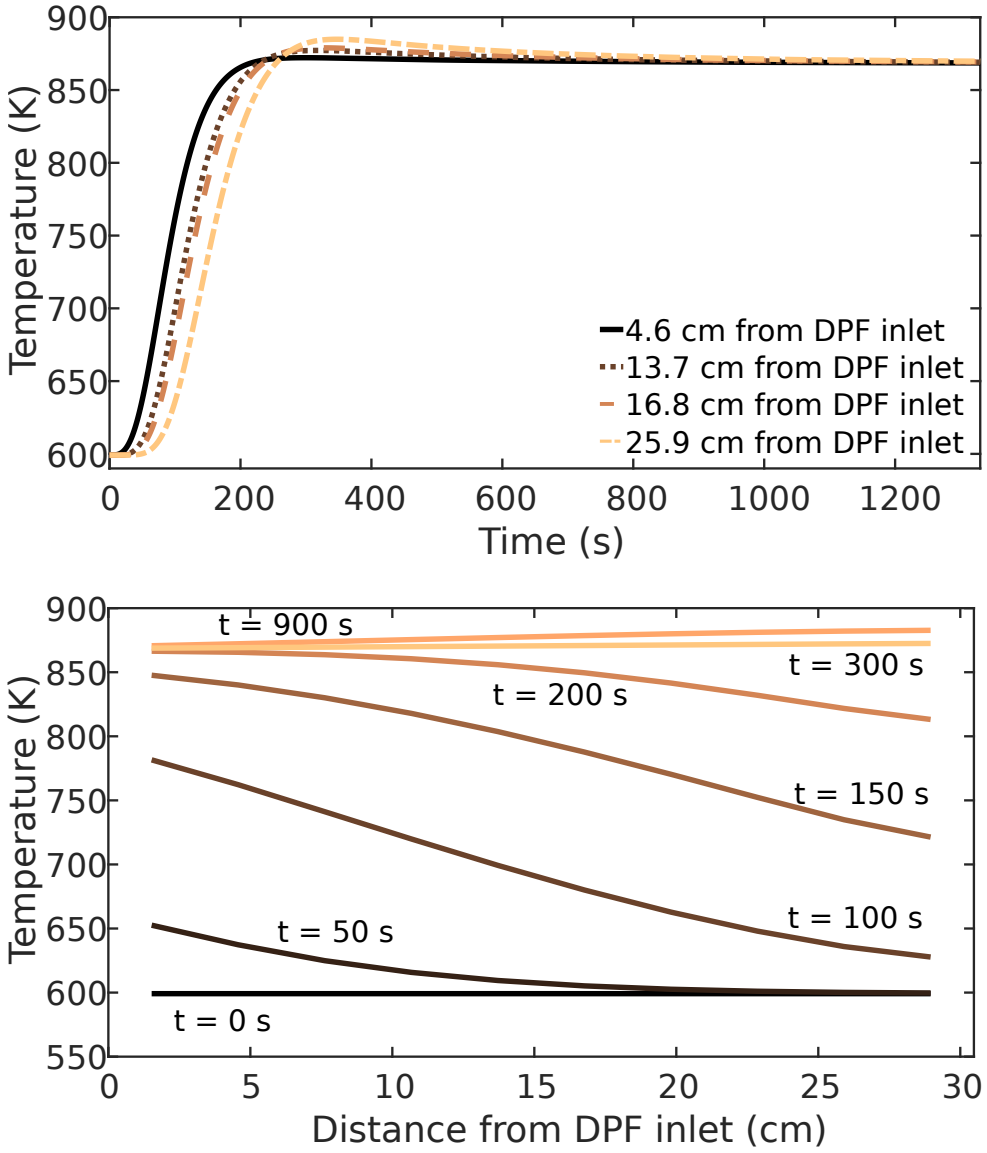

Figure S5: *Simulated DPF wall temperature during regeneration.*